Paper Number: **189**

Session Topic: **Special Session Honoring the Contributions of Dr. T Kevin O'Brien, NASA Langley Research Center**

Title: **Study of Skin-Stringer Separation in Postbuckled Composite Aeronautical Structures**

Authors: Lucas J. Kootte
Chiara Bisagni
Carlos G. Dávila
Vipul Ranatunga

ABSTRACT

Aeronautical composite stiffened structures have the capability to carry loads deep into postbuckling, yet they are typically designed to operate below the buckling load to avoid potential issues with durability and structural integrity. Large out-of-plane postbuckling deformation of the skin can result in the opening of the skin-stringer interfaces, especially in the presence of defects, such as impact damage. To ensure that skin-stringer separation does not propagate in an unstable mode that can cause a complete collapse of the structure, a deeper understanding of the interaction between the postbuckling deformation and the development of damage is required. The present study represents a first step towards a methodology based on analysis and experiments to assess and improve the strength, life, and damage tolerance of stiffened composite structures subjected to postbuckling deformations.

Two regions were identified in a four-stringer panel in which skin-stringer separation can occur, namely the region of maximum deflection and the region of maximum twisting. Both regions have been studied using a finite element model of a representative single-stringer specimen. For the region of maximum deflection, a seven-point bending configuration was used, in which five supports and two loading points induce buckling waves to the specimen. The region of maximum twisting was studied using an edge crack torsion configuration, with two supports and two loading points. These two configurations were studied by changing the positions of the supports and the loading points. An optimization procedure was carried out to minimize the error between the out-of-plane deformation of the representative single-stringer specimen and the corresponding region of the four-stringer panel.

Lucas J. Kootte, Delft University of Technology, Faculty of Aerospace Engineering, 2629HS Delft, Netherlands

Chiara Bisagni, Delft University of Technology, Faculty of Aerospace Engineering, 2629HS Delft, Netherlands

Carlos G. Dávila, NASA Langley Research Center, MS190, Structural Mechanics and Concepts Branch, Hampton, VA 23681, USA

Vipul Ranatunga, Air Force Research Laboratory, Wright-Patterson AFB, OH 45433, USA

INTRODUCTION

Aeronautical composite stiffened structures are typically designed to operate at loads below the buckling load to ensure durability and structural integrity. The interaction of complex failure modes, which is inherent to composites, in combination with the large out-of-plane displacement of the skin associated with buckling, can result in skin-stringer separation. To design aeronautical structures that can operate in postbuckling without the possibility of unstable skin-stringer separation, a deeper understanding of the interactions between structural and material response is necessary. This knowledge must be based on a more precise material and structural characterization that can only be achieved using a combination of advanced numerical methods and experimental evaluations of specialized structural sub-elements.

A number of studies can be found in the literature on simplified structural specimens that are representative of critical loading conditions in a postbuckled stiffened panel. The three-point bending test, in which out-of-plane deformation is applied to a specimen with a skin and a co-bonded or co-cured doubler, is representative of the opening mode of a stringer flange disbond [1-2] that results from a combination of the high deflection of the skin and the mismatch in flexural stiffness of the skin and stringer. A similar type of damage has also been investigated using a seven-point bending (7PB) test, which adds the complex interaction of the buckling deformation of the skin [3-5]. The 7PB test consists of a single-stringer specimen supported at five points and loaded at two points such that the out-of-plane deformation of the skin is similar to a half-wave section of a postbuckled multi-stringer panel. Another test that represents the postbuckling deformation of a multi-stringer panel is the single-stringer compression test [6-10], which accounts for the in-plane compressive stresses.

In all of these tests, debonding of the skin-stringer is dominated by mode I loading, representing the location where the deflection due to the buckling wave is at its maximum. However, research on skin-stringer separation indicates that a possible combined mode II + III failure can also be a critical mode of failure due to the twisting of the skin at the inflection point, located in between two buckling half-waves [5, 9]. Inflection points can be critical locations, for example, in structures with a tapered stringer flange termination, where a relatively low bending stiffness mismatch between the skin and stringer flange reduces the likelihood of separation in mode I.

The objective of the present work is to develop a methodology to design an experimental capability that can be used to evaluate the different critical locations in postbuckled composite multi-stringer panels where skin-stringer separation may occur. The first goal of this effort is to develop structural sub-elements that approximate the multi-stringer panel response of these critical locations and are less expensive to manufacture and test than the corresponding multi-stringer panel. Analysis of sub-elements is also computationally less demanding than analyses of larger structures, which allows the use of finer meshes to investigate the performance of detailed damage models that can predict skin-stringer separation. In addition, sub-elements can be more easily examined in detail experimentally to characterize details of damage development growth.

The postbuckling deformation of a four-stringer panel was investigated and two critical regions of the panel were identified. Two sub-element specimens representing

these critical locations were designed. The first sub-element is representative of the region of the four-stringer panel with maximum out-of-plane skin deflection. This deformation mode, which promotes opening of the skin-stringer interface, was studied using a representative single-stringer specimen in a 7PB configuration. The second specimen is representative of the region around an inflection point in the postbuckled deformation of the four-stringer panel and was studied using a single-stringer specimen in an edge crack torsion (ECT) configuration, where two supports and two loading points were used to create a twisting deformation on the specimen [11-13]. Different loading conditions of these configurations were obtained by varying the positions of the supports and loading points. The out-of-plane deformation of the specimen for each condition was compared to the shape of the postbuckling deformation of the corresponding region of the four-stringer panel.

FOUR-STRINGER PANEL

The postbuckling deformation of a four-stringer panel subjected to in-plane compression loading was analyzed. The geometry and the dimensions of the panel and stringer are shown in Figure 1. The center skin bay is 108-mm wide and the exterior bays are 102-mm wide, which ensures that the skin in the center bay buckles before the exterior bays. The skin and stringers are made of unidirectional graphite-epoxy IM7/977-3. The stacking sequence for the skin and stringers is quasi-isotropic: $[-45/45/0/90/-45/45]_s$. The resulting symmetric lay-up for the skin, the stringer, and the skin-stringer overlap minimize the residual stresses that develop during manufacturing. The material properties of IM7/977-3 are reported in Table I [14].

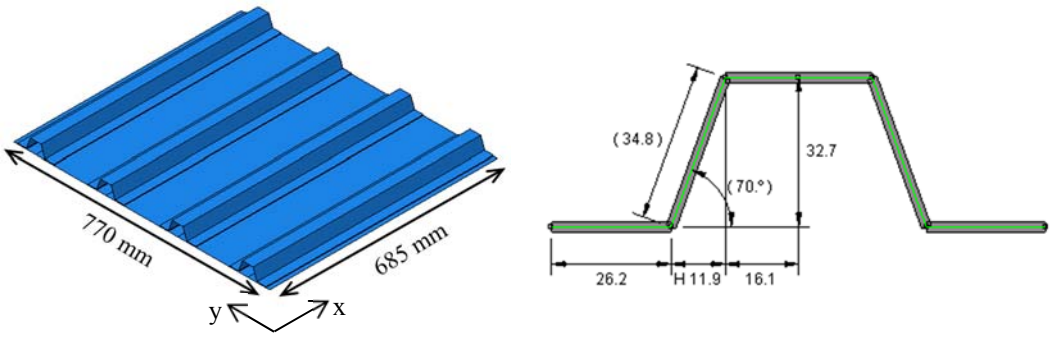

Figure 1. Four-stringer panel: geometry and stringer dimensions in mm.

TABLE I. MATERIAL PROPERTIES OF IM7/977-3

Ply Thickness (mm)	E_{11} (GPa)	E_{22} (GPa)	G_{12} (GPa)	G_{13} (GPa)	G_{23} (GPa)	ν_{12}
0.127	164	8.98	5.01	5.01	3.0	0.32

A finite element (FE) model of the four-stringer panel was built in Abaqus 2017 to investigate the out-of-plane deformation due to buckling. The skin and stringer were discretized using a 5 mm by 5 mm mesh consisting of conventional shell elements (S4R). These computationally efficient elements capture well the nonlinear

response of thin structures subjected to large deformations. The skin and stringers are clamped at both ends of the panel and an in-plane end-shortening is applied. The first buckling mode of the panel predicted by eigenvalue analysis occurs at an applied displacement of 0.6 mm and a force of 96 kN. The buckling eigenmode is shown in Figure 2.

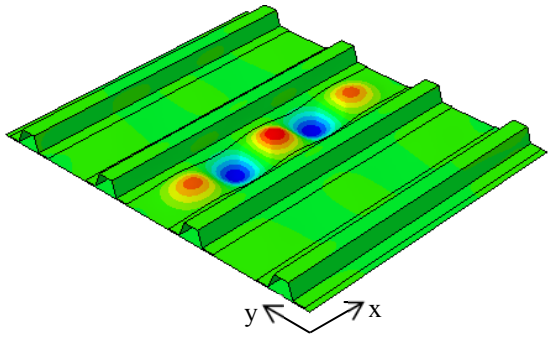

Figure 2. First buckling mode of four-stringer panel.

The force-displacement curve of the panel is obtained using a nonlinear solver. The result is shown in Figure 3, together with the out-of-plane displacement field corresponding to an in-plane applied displacement of 2 mm. At this applied displacement, all three bays of the panel have buckled.

Two areas are highlighted on the panel, namely region 1 and region 2. Region 1 consists of a buckling full wave on each side of the stringer centered around the locations of the maximum out-of-plane deflection. Region 2 encloses an inflection point of the buckling wave on each side of the stringer. FE models of single-stringer specimens that are representative of these two regions were developed.

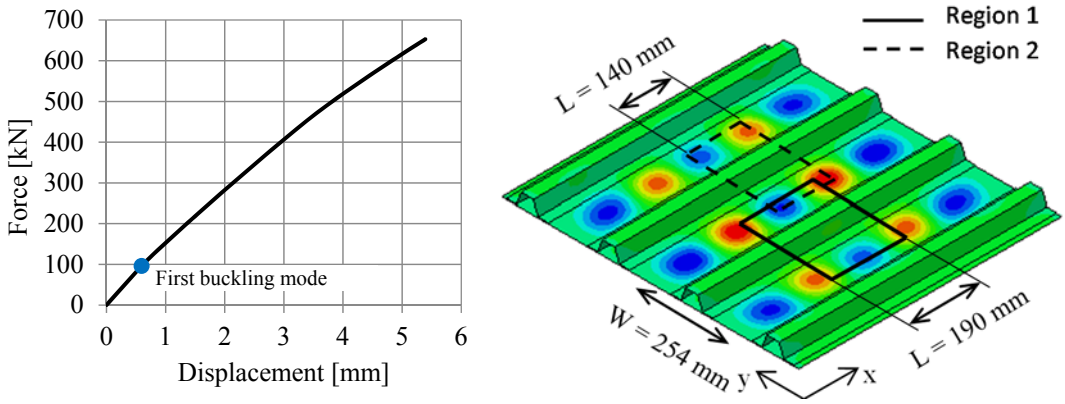

Figure 3. Quasi-static analysis of four-stringer panel: force-displacement response and contour plot of out-of-plane displacement at an applied end-shortening displacement equal to 2 mm.

REGION 1

The out-of-plane deformation of region 1 in the four-stringer panel was approximated using a single-stringer specimen in a 7PB configuration, as illustrated in Figure 4. The specimen was modeled using S4R elements. The boundary

conditions consist of five lower supports and two upper loading points. Each load and boundary condition was applied to a single node in the FE model. The out-of-plane displacement of the support nodes was constrained and an out-of-plane displacement was applied to the nodes corresponding to the loading points.

The model was used to perform a parametric study to find the optimum loading condition of the 7PB configuration that best represents the deformation of the corresponding location on the four-stringer panel. The distances S_X and S_Y define the positions of the corner supports, and L_X and L_Y are the longitudinal and transverse distances to the edge of the skin that define the locations of the loading points.

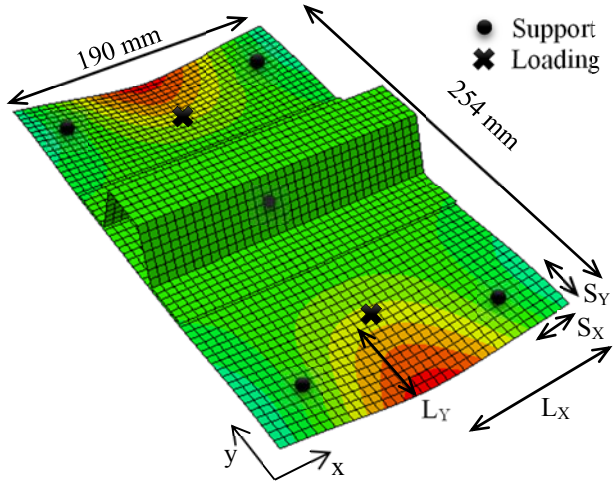

Figure 4. Seven-point bending configuration.

The following design constraints were imposed to the four position variables. The corner supports and the loading points must be at least 20 mm away from the edges of the specimen to ensure that the stress concentrations at the free edge are limited ($S_X \geq 20$ mm, $S_Y \geq 20$ mm and $L_Y \geq 20$ mm). The corner supports and loading points are placed symmetrically along both axes ($L_X = 95$ mm). The distance S_X is taken equal to 27 mm, because this is the position of the inflection line between the half-waves in region 1 of the four-stringer panel. The fifth support is positioned at the center of the specimen. With these constraints, the configuration is defined by two independent variables, S_Y and L_Y.

The out-of-plane displacements of the single-stringer specimen in the different 7PB loading conditions were compared with the out-of-plane displacement of region 1 of the four-stringer panel using the residual sum of squares (RSS) method. The condition that results in the lowest RSS corresponds to the best approximation to the desired deformation. The equation for RSS is given by:

$$RSS = \sum_{i=1}^{n} \left(y_i - f(x_i)\right)^2 \tag{1}$$

where y_i is the nodal out-of-plane displacement in region 1 and $f(x_i)$ is the corresponding out-of-plane displacement of the 7PB specimen. For the 7PB configuration, the RSS surface is plotted as a function of the variables S_Y and L_Y in

Figure 5. For the 7PB configuration, a total of 17 iterations were investigated to find the loading condition with the lowest RSS.

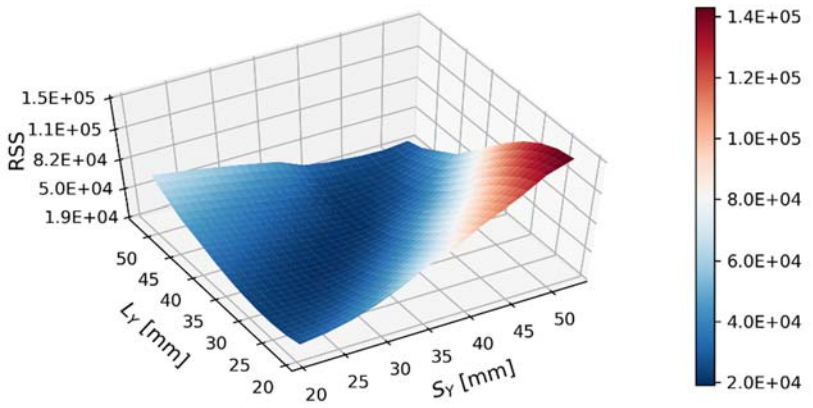

Figure 5. Surface plot of RSS for region 1 as a function of variables S_Y and L_Y.

The out-of-plane displacement for region 1 is shown in Figure 6 together with the results for the 7PB specimen for three different sets of values of the variables S_Y and L_Y. Increasing L_Y results in a higher gradient of the deflection between the flange and the loading point. Increasing S_Y results in a wider buckling wave towards the edge of the skin. The results of 17 iterations indicate that the loading conditions with S_Y equal to 37 mm and L_Y equal to 37 mm corresponds to the lowest RSS. For this model, the applied transverse displacement at the loading points is 3.8 mm, which corresponds to a total loading force of 1.1 kN.

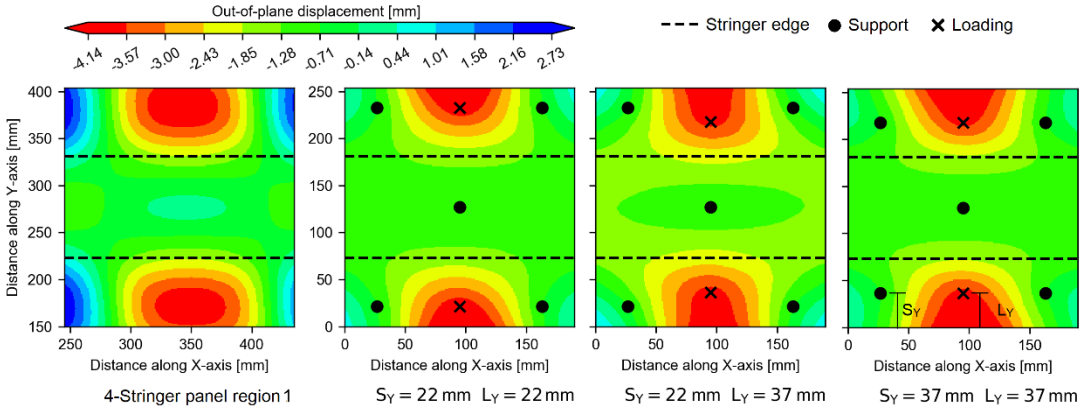

Figure 6. Contour plots of the skin out-of-plane displacement at an applied in-plane displacement equal to 2 mm: for region 1 of the four-stringer panel and for three different configurations of the 7PB specimen.

To verify whether this configuration can be used to approximate the deformation in region 1 at a higher in-plane compressive displacement of the four-stringer panel, a second comparison was performed at an applied in-plane displacement of 5 mm. This applied displacement corresponds to an axial compression of 7300 microstrain, which is somewhat higher than the expected failure of the panel. The deformation shapes for both region 1 and the 7PB configuration are shown in Figure 7. In this 7PB

configuration, the displacement of the loading points is 5.6 mm, with a corresponding total force of 1.9 kN. Since no mode changes occurred in the four-stringer panel between the applied in-plane displacements of 2 mm and 5 mm, the configuration of 7PB remains representative of the response of region 1 of the panel between the onset of buckling (applied displacement of 2 mm) and expected failure (applied displacement below 5 mm).

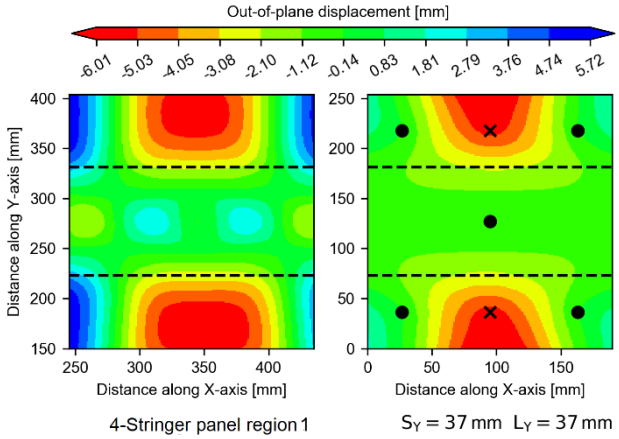

Figure 7. Contour plots of the skin out-of-plane displacement at an applied in-plane displacement equal to 5 mm: for region 1 of the four-stringer panel and for the 7PB specimen.

REGION 2

The twisting deformation of region 2 in the four-stringer panel was approximated using a single-stringer specimen in an edge crack torsion configuration, where two lower supports and two upper loading points, positioned diagonally from each other, were used to apply torsion to the specimen, as illustrated in Figure 8. A model of a single-stringer specimen was constructed with S4R elements. The variables for the ECT configuration are S_X and S_Y distances for the position of the supports and L_X and L_Y for the position of the loading points.

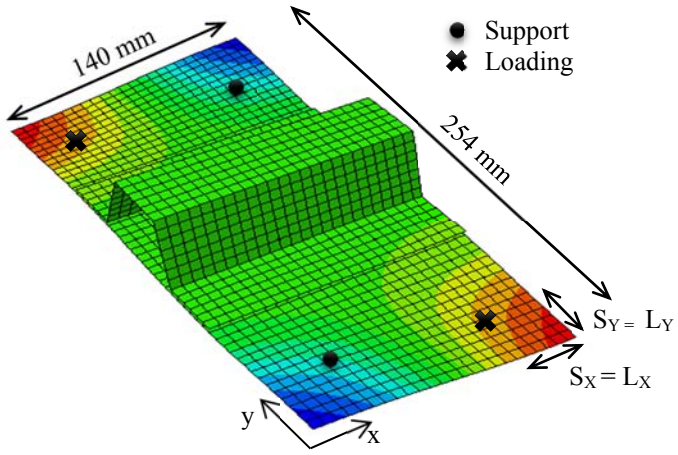

Figure 8. ECT test configuration.

The number of variables was reduced by imposing the following constraints to the configuration. First, the loading points and the supports are equidistant from the free edges ($S_X = L_X$ and $S_Y = L_Y$). Secondly, the distance between the loading points to the free edges of the specimen must be greater than 20 mm ($S_Y \geq 20$ mm and $L_Y \geq 20$ mm). Therefore, the configuration of the ECT test is defined by the two independent variables S_X and S_Y. The postbuckling deformation in region 2 of the four-stringer panel is symmetric with respect to the longitudinal axis, whereas the ECT test configuration imposes an anti-symmetric deformation with respect to the longitudinal stringer axis. Therefore, the response of only half of the ECT specimen is compared against the corresponding region in the four-stringer panel. A total of 35 iterations were carried out to obtain the loading condition with the lowest RSS. The RSS surface as a function of these two variables is plotted in Figure 9.

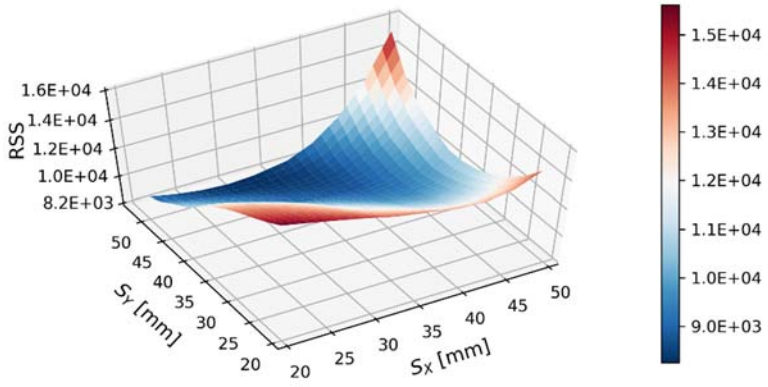

Figure 9. Surface plot of RSS for region 2 as a function of variables S_Y and S_X.

The out-of-plane deformation of region 2 in the four-stringer panel is compared in Figure 10 to the out-of-plane displacement of the single-stringer specimen with three different conditions of the ECT configuration. Increasing S_Y causes a higher gradient in the out-of-plane displacement between the stringer flange and the loading point. Increasing S_X results in a higher gradient between the support and loading point. From these 35 iterations, the configuration with $S_X = 34$ mm and $S_Y = 48$ mm resulted in the lowest RSS. In this loading condition, the displacement of the two loading points is 5.1 mm, which corresponds to a total applied force of 1.0 kN.

To verify whether this configuration can be used to represent the deformation of region 2 of the four-stringer panel at a higher applied in-plane compressive displacement, the analyses were repeated with an in-plane displacement equal to 5 mm. The deformation shapes for region 2 and the ECT configuration are shown in Figure 11. In this ECT configuration, the displacement of the loading points is 9.8 mm and the corresponding total force is 2.8 kN. Since no buckling mode changes occur in the four-stringer panel between the onset of buckling at an applied displacement of 2 mm and expected failure at an applied displacement of 5 mm, the configuration of the ECT remains representative of the response of region 2 of the four-stringer panel.

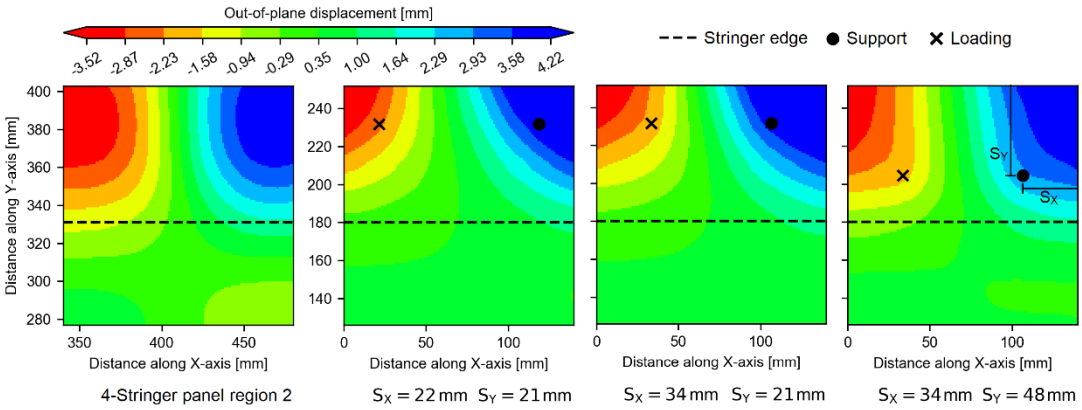

Figure 10. Contour plots of the skin out-of-plane displacement at an applied in-plane displacement equal to 2 mm: for region 2 of the four-stringer panel and for three different configurations of the ECT single-stringer specimen.

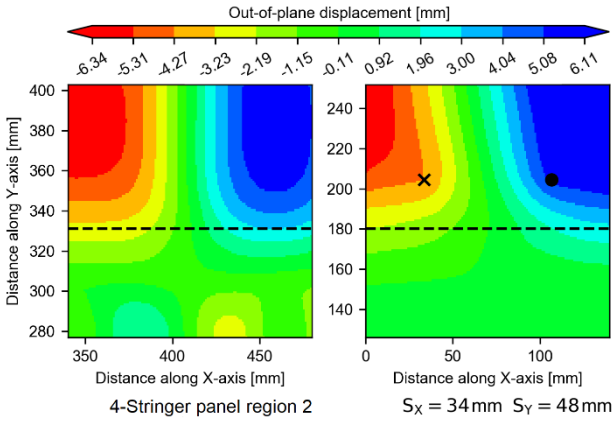

Figure 11. Contour plots of the skin out-of-plane displacement at an applied in-plane displacement equal to 5 mm: for region 2 of the four-stringer panel and of the ECT single-stringer specimen.

CONCLUDING REMARKS

The first steps to the development of a methodology for the study of the skin-stringer separation in composite structures is described in this paper. The first goal of this effort was to develop structural sub-elements that are less expensive to manufacture and test than the corresponding multi-stringer panel. Because these sub-elements are intended to be tested under out-of-plane displacement control and for specific loading conditions, they can potentially provide a more precise substantiation of the durability and damage tolerance of individual modes of failure in a multi-stringer panel. Finally, sub-element specimens require analysis models that are computationally less demanding than larger specimens. Therefore, these smaller models are more suitable for the development and validation of damage models that can accurately predict skin-stringer separation.

The buckling deformation of a four-stringer panel loaded in compression was analyzed and two critical deformation regions were identified. The first region, where the out-of-plane deflection of the skin is at its maximum, was approximated with the

use of single-stringer specimen in a seven-point bending configuration, in which five supports and two loadings points impose an out-of-plane deformation. The second region, characterized by twisting of the skin, was approximated using an edge crack torsion configuration, in which two supports and two loading points apply out-of-plane displacements. The optimal position of the supports and loading points for these configurations were determined by minimizing the difference between the out-of-plane displacement of the single-stringer configurations and the out-of-plane displacement in corresponding regions in the four-stringer panel.

The next step in this effort will be to verify that skin-stringer separation in the single-stringer specimens in the two configurations outlined is similar to the separation of the corresponding region in the four-stringer panel. The development of skin-stringer interface damage will be investigated using a cohesive-based model. The models will then be validated by comparing the predicted results with the experimental results of these 7PB and ECT test configurations.

ACKNOWLEDGEMENTS

The first two authors gratefully acknowledge the financial support received from the European Office of Aerospace Research and Development (EOARD), United States Air Force, under the guidance of Dr. David Garner.

REFERENCES

1. P.J. Minguet and T.K. O'Brien. 1996. "Analysis of Test Methods for Characterizing Skin-Stringer Debonding Failures in Reinforced Composite Panels," in *Composite Materials: Testing and Design: Twelfth Volume*. ASTM International.
2. C.G. Dávila, F.A. Leone, K. Song, J.G. Ratcliffe, and C.A. Rose. 2017. "Material Characterization for the Analysis of Skin/Stiffener Separation," in Proceedings of the *32nd American Society for Composites Conference,* West Lafayette, IN.
3. J.C.F.N. van Rijn and J.F.M. Wiggenraad. 2000. "A Seven-Point Bending Test to Determine the Strength of the Skin-Stiffener Interface in Composite Aircraft Panels," *NLR-TP2000-044, National Aerospace Laboratory (NLR).*
4. J. Bertolini, B. Castanié, J.J. Barrau, J.P. Navarro, and C. Petiot. 2009. "Multi-Level Experimental and Numerical Analysis of Composite Stiffener Debonding. Part 2: Element and Panel Level," *Composite Structures*, 90(4):392-403.
5. S. Wanthal, J. Schaefer, B. Justusson, I. Hyder, S. Engelstad and C. Rose. 2017. "Verification and Validation Process for Progressive Damage and Failure Analysis Methods in the NASA Advanced Composites Consortium," in Proceedings of the *32nd American Society for Composites Conference*, West Lafayette, IN.
6. C. Bisagni. 2006. "Progressive Delamination Analysis of Stiffened Composite Panels in Post-Buckling," Proceedings of the *47th AIAA/ASME/ASCE/ASC Structures, Structural Dynamics, and Materials Conference,* AIAA Paper 2006-2178.
7. D. C. Jegley. 2009. "Experimental Behavior of Fatigued Single Stiffener PRSEUS Specimens," *Technical Publication NASA/TM-2009-215955*.
8. C. Bisagni, R. Vescovini, and C.G. Dávila. 2011. "Single-Stringer Compression Specimen for the Assessment of Damage Tolerance of Postbuckled Structures," *Journal of Aircraft*, 48(2):495-502.
9. R. Vescovini, C.G. Dávila, and C. Bisagni. 2013. "Failure Analysis of Composite Multi-Stringer Panels using Simplified Models," *Composites Part B: Engineering*, 45(1):939-951.
10. C. Bisagni and C.G. Dávila. 2014. "Experimental Investigation of the Postbuckling Response and Collapse of a Single-Stringer Specimen," *Composite Structures*, 108:493-503.

11. J. Li, S.M. Lee, E.W. Lee, and T.K. O'Brien. 1997. "Evaluation of the Edge Crack Torsion (ECT) Test for Mode III Interlaminar Fracture Toughness of Laminated Composites," *Journal of Composites, Technology and Research*, 19(3):174-183.
12. A.B. De Morais, A.B. Pereira, M.F.S.F. De Moura, and A.G. Magalhães. 2009. "Mode III Interlaminar Fracture of Carbon/Epoxy Laminates using the Edge Crack Torsion (ECT) Test," *Composites Science and Technology*, 69(5):670-676.
13. M.W. Czabaj, J.G. Ratcliffe, and B.D. Davidson. 2014. "Observation of intralaminar cracking in the edge crack torsion specimen," *Engineering Fracture Mechanics*, 120: 1-14.
14. S.B. Clay, and P.M. Knoth. 2017. "Experimental Results of Quasi-Static Testing for Calibration and Validation of Composite Progressive Damage Analysis Methods," *Journal of Composite Materials*, 51(10): 1333-1353.